The Use of Platelet-Rich Fibrin Coated 3d Printed Scaffolds in Salvage of Complex Hindfoot Cases

Ken Meng Tai *, Justin Mooteeram, Anand Pillai *

Posted Date: 1 April 2025

doi: 10.20944/preprints202504.0044.v1

Keywords: 3D printed implant; 3D printed scaffold; hindfoot fusion; talar defect; RIA; AVN talus; PRF; Platelet-rich fibrin; bioactive matrix

 doi:10.20944/preprints202504.0044.v1

Article

The Use of Platelet-Rich Fibrin Coated 3d Printed Scaffolds in Salvage of Complex Hindfoot Cases

Ken Meng Tai *, Justin Mooteeram and Anand Pillai

Wythenshawe Hospital, Manchester University NHS Foundation Trust (MFT), Southmoor Rd, Wythenshawe, Manchester M23 9LT, UK

* Correspondence: kenmeng85@hotmail.com

Abstract: Background: Complex hindfoot pathologies involving critical sized bone defects of talus are difficult to manage. The current management involves arthrodesis and bone grafting with the defective talus which have limitations in restoring structural integrity and functional goals. The advancement of 3D printed scaffolds have opened new avenues to address such complex hindfoot pathologies which may potentially improve treatment outcomes. The addition of Platelet-rich fibrin further enhances healing potential. **Method:** This is a retrospective study involving 6 patients with severe hindfoot bone loss where 3D printed scaffolds coated with PRF were performed as a salvage surgery from 2023 to 2024. We intend to to investigate the clinical outcomes in terms of healing time and union rate. Additionally we would evaluate the degree of deformity corrections and patient clinical outcomes. **Results:** This report includes 6 complex reconstructions where all the patients (100%) achieved CT confirmed union with mean duration of 20.2 weeks. All patients were able to ambulate in full weight bearing after an average duration of 23.3 weeks. There were significant improvement in all radiological parameters. Patients demonstrated improved VAS from 7.5 ± 1.4 points to 2.3 ± 1.2 and functional scores in all domains utilizing AOFAS score, FFI and SF-36. **Conclusion:** This demonstrated the potential of PRF coated 3D printed scaffold in managing complex hindfoot cases especially in the presence of significant bony defects. This modality demonstrated excellent union rate of 100%, near anatomical correction and good functional outcomes with low complication rate.

Keywords: 3D printed implant; 3D printed scaffold; hindfoot fusion; talar defect; RIA; AVN talus; PRF; Platelet-rich fibrin; bioactive matrix

1. Introduction

The hindfoot which consists of the talus, calcaneus and the surrounding soft tissue encompasses 3 important joints namely subtalar, talonavicular and calcaneocuboid joints. This complex structure plays a crucial role in shock absorption, weight bearing, gait cycle and affects function of surrounding joints [1]. The rate of hindfoot pathologies is increasing along with the improving life expectancy with a reported 13.4% of adults over the age of 50 years old experienced hindfoot pain [2]. Complex hindfoot pathologies which arise due to serious trauma, infection such as osteomyelitis and septic arthritis, avascular necrosis, degenerative arthritis and failed reconstructive surgeries entails formidable challenges to the orthopedic fraternity.

Talar deformity with associated bone loss is particularly arduous to manage. Talus integrity is crucial in maintaining hindfoot alignment and midfoot position through the transverse tarsal joint, constituting a complex geometrical and biomechanical structure required for proper locomotion. Due to its innate lack of periosteal coverage, delicate blood supply, absence of muscular attachment and with majority of surface enveloped by hyaline cartilage due to multiple joint articulations, it is susceptible to avascular necrosis (AVN) or osteonecrosis [3]. The prognosis of talar fracture is relatively poor despite surgical management with reported overall incidence of AVN in 26.5 to 65%,

 doi:10.20944/preprints202504.0044.v1

ankle arthritis in 51.7 to 98.0% and subtalar arthritis in 45.0% of cases [4,5]. The long term outcome of talus fracture after surgical treatment was reported to be moderate in terms of pain and disability score with up to 41% of patients not able to return to their daily activities [6].

Infection is another common cause of complex hindfoot pathologies. Septic arthritis causes significant articular cartilage damage due to loss of chondrocyte. It has been demonstrated that 10 years survival of a native knee joint after an episode of septic arthritis was 65.5% suggesting a secondary degenerative process [7]. Presence of osteomyelitis significantly worsen the prognosis with direct bone damage caused by pathogens or radical debridement including bone resection to treat this condition leading to bone loss and altered mechanical integrity. They are also associated with multiple large cystic lesion with possibility of collapse which further limit surgical options [8]. Osteomyelitis of the hindfoot is reported to be associated with transtibial amputation in up to 52.2% [9].

The common practice in managing complex hindfoot pathologies involves an arthrodesis which may involve osteotomies, removal of articular cartilage, bone grafting and fixation with plate, screws, nail or external fixator device. Such methods often fall short due to failure in addressing patient specific deformities. This may lead to complications such as failure of correction, recurrence, implant failure and limb length discrepancy in addition to arthrodesis associated complications which includes nonunion, malunion, infection, hardware breakage or loosening and amputation [10]. A recent systemic review on computed tomography scan confirmation of union reported an overall union rate of ankle arthrodesis of only 78.7% [11]. The occurrence of deformity is common after hindfoot fusion with reported valgus tibiotalar tilt of up to 27% [12]. Such complication is detrimental and may lead to impingement, adjacent joint arthritis and implant failure.

The emergence of 3D printing, also known as additive manufacturing opens up avenues in dealing with such complex hindfoot cases especially in the presence of bone voids. This layer by layer process allows manufacturing of scaffolds that specifically match patients' unique deformity allowing optimal fit and mechanical stability. The use of titanium alloys which is biocompatible provide sufficient compressive strength and corrosive resistance that is suitable for load bearing device, reportedly achieving similar elastic module to native bone [13]. Additionally 3D printing grant complex customization of implant design while integrating porous structure and pattern which promotes bone in-growth and integration [14]. It has been well established that porous implants with size of 1000 µm achieved significantly better fusion rate in terms of vascularization and osteointegration compared to 500 µm and non porous designs [15]. The roughened outer surfaces which is coupled to bone promotes osteoblast adhesion which promotes osteointegration.

3D-printed cages are particularly useful in managing critical sized bone defects, typically defined as defects more than 2.5 cm or 50% of circumference of the involved bone as it will not achieve union even with surgical stabilization [16]. The process of constructing such custom made implants involves surgeons input and the expertise of bioengineers to match the defect size anatomically. This allows enhanced precision during surgery and reduce surgical time which translates to better cost effectiveness. Despite still being in its early stages, studies have reported good union rate with the use of 3D-printed cages for severe bone loss in foot and ankle cases, with 87% of patients reported substantial pain and functional improvement [17].

There is however potential barriers to this new device with a study reporting 33.3% of cases required a second surgery and 25.6% necessitated removal of implants due to nonunion [18]. A systematic review involving spinal surgeries demonstrated subsidence of more than 3mm in 11 out of 35 patients [19]. With the scarcity of long term studies of 3D printed implant, there are concerns regarding osteointegration, wound healing, infection, rejection and allergic response. Platelet-rich fibrin (PRF) which is derived from patient's own blood is autologous and biocompatible, rich in bioactive factors which could improve osteointegration and union rate [20]. Autologous PRF produced by the Vivostat device was reported to have additional advantages in integration of tissues and ability coat implants while maintaining matrix integrity for up to 4 weeks [21]. This allows the use of antibiotics and additional bone graft to be packed safely within the 3D printed cage.

 doi:10.20944/preprints202504.0044.v1

This present study intends to evaluate clinical, radiological and functional outcomes of patients who underwent salvage surgery with PRF coated 3D-printed scaffolds in complex hindfoot cases. We would also like to share our experience in the design and surgical process of this relatively new procedure.

2. Materials and Methods

This is a retrospective study involving 6 patients with complex hindfoot deformities surgically treated with PRF coated 3D-printed scaffolds in Wythenshawe Hospital, Manchester University Foundation Trust from 2023 to 2024. There were no exclusion criteria. All procedures were performed by a single board certified Foot and Ankle consultant. Implants were manufactured by Meshworks®, UK which conforms to Medical Devices Directive 93/42 EEC (UK MDR 2002) and Medical Device Regulations (MDR 2017/745). PRF matrix utilized were ArthroZheal®, prepared and applied through the Vivostat® System (TRB Chemedica, UK).

2.1. Preoperative Planning

CT scan were performed for surgical planning to determine size and degree of defect and severity of deformity to assist in the implant design. An online teleconference between the surgical team, Meshworks design engineer and implant distributor was performed to discuss required resection, correction aim and implant design, configuration and position with 3D visualization. Auxiliary plastic guides that assist in bone resection and specific characterization of cage which includes screw amount and direction is mapped at this point. Implant design finalization was done before manufacturing which will take approximately 2 weeks before delivery for sterilization. (Figures 1–4)

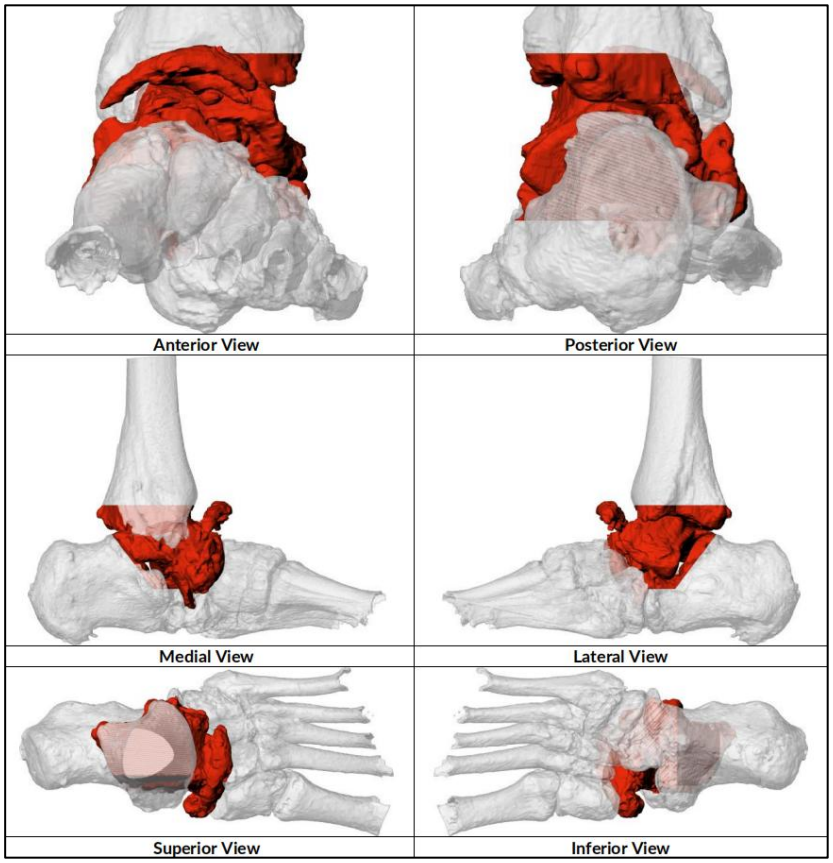

Figure 1. Preoperative Resection Planned for Implant Design.

Preprints.org (www.preprints.org) | NOT PEER-REVIEWED | Posted: 1 April 2025 doi:10.20944/preprints202504.0044.v1

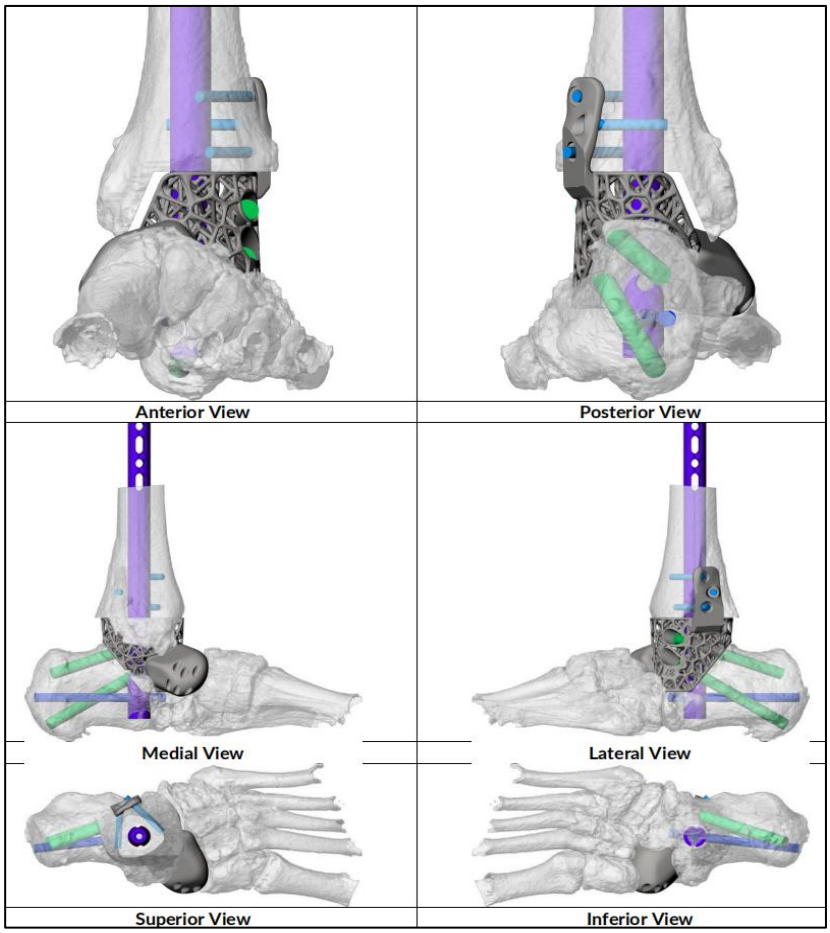

Figure 2. Preoperative Reconstruction with Implant Position.

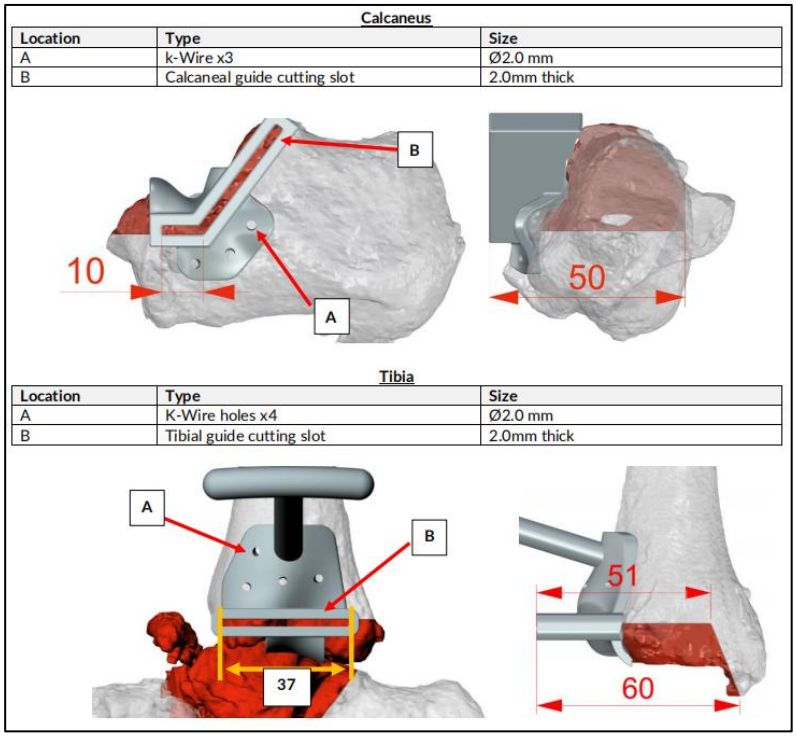

Figure 3. Preoperative Plan of Plastic Guides for Resection of Distal Tibia and Calcaneum.

 doi:10.20944/preprints202504.0044.v1

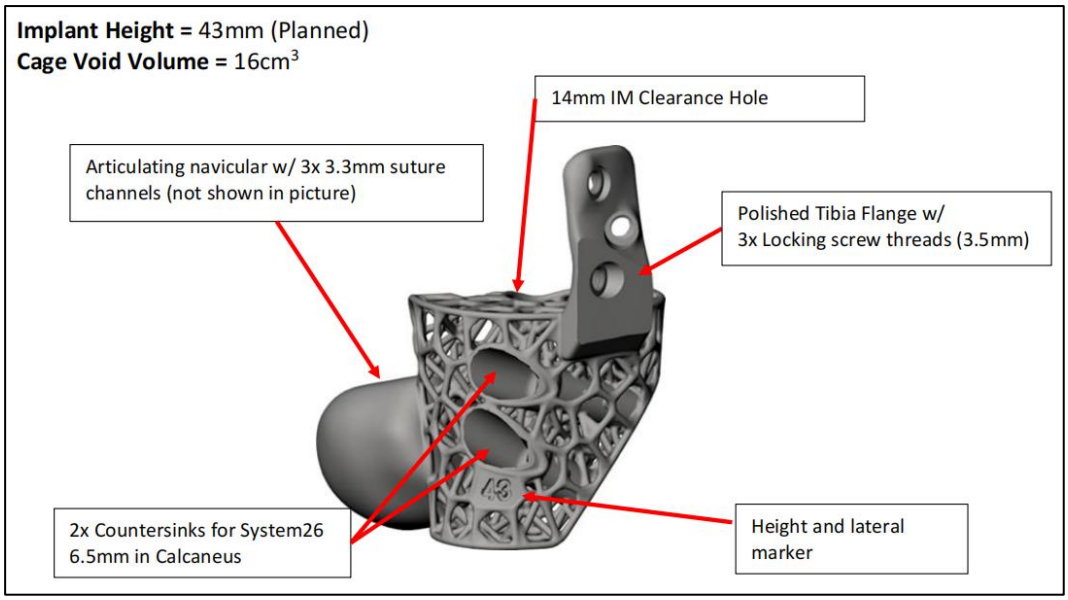

Figure 4. Finalised Implant Design.

2.2. Surgical Technique

The procedures were performed under general anesthesia with peripheral blocks. Prophylactic antibiotics (Teicoplanin and Gentamicin) were delivered during induction. The patients were first positioned supine on a radiolucent traction table for Reamer-Irrigator-Aspirator (RIA) procedure to obtain sufficient autologous bone graft. They will then be repositioned in supine on radiolucent table with foot at the lower end of the table. High thigh tourniquet were applied and inflated after standard prepping and draping. Surgical approaches were dependent on previous scar, major pathological side and additional deformities which may require supplementary incisions. Talectomy were performed and bony resection of distal tibia and calcaneum were done based on preoperative planning. Bony resection were completed with the help of specific auxiliary guide matching implant geometry. (Figure 5) Trials were performed with 3 sizes of provided 3D-printed trial blocks and the best positionally fitting one were chosen. (Figure 6) Wound washout were done followed by multiple drill holes insertion at fusion sites with K-wires for improved osteointegration.

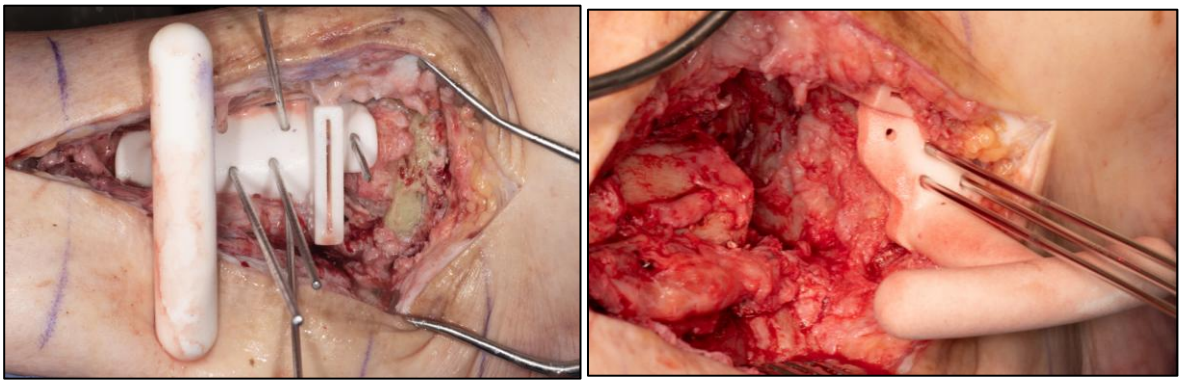

Figure 5. Bony Cuts performed through Plastic Guides.

 doi:10.20944/preprints202504.0044.v1

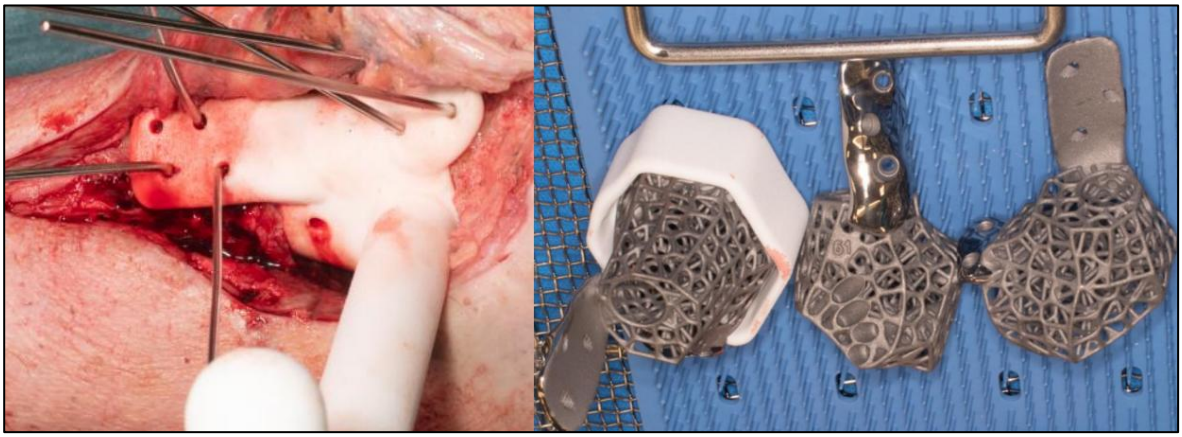

Figure 6. Trial Performed with Trial Blocks with 3 different Size of Cages Available.

For implants that incorporate the hindfoot nail, the guidewire were passed through the calcaneus into a cylindrical hole on the 3D trial block to the tibia before reaming in ascending sizes were performed. The chosen 3D printed keystone talus cage were filled with autologous bone graft harvested from RIA. Arthrozheal were then applied to the surface of keystone talus with the Vivostat® Applicator Unit. (Figures 7 and 8) The nail guidewire were removed and the keystone talus were then inserted into the prepared space. Guidewire were reinserted followed by insertion of desired tibiotalocalcaneal nail (Oxbridge ankle fusion nail) while maintaining optimum hindfoot position. Proximal locking screws were performed through the holes of the hindfoot nail. Further compression were performed through attachment of the jig through the nail to improve bony interface before insertion of distal locking screws through the calcaneum. Additional screws were inserted from the cage into the calcaneum when necessary. Locking screws were supplemented to implants which incorporated tibial or navicular flanges. Wounds were closed in layers followed by sterile dressing, padding and application of below knee cast.

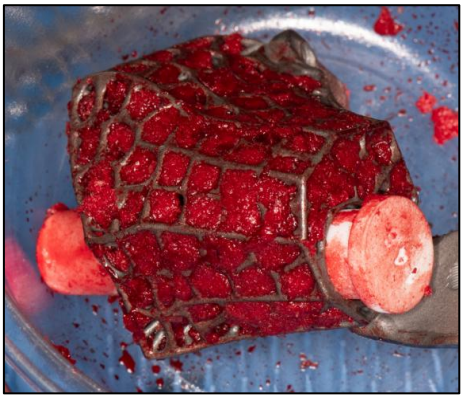

Figure 7. Cage filled with Autologous Bone Graft from RIA followed by Application of Arthrozheal.

 doi:10.20944/preprints202504.0044.v1

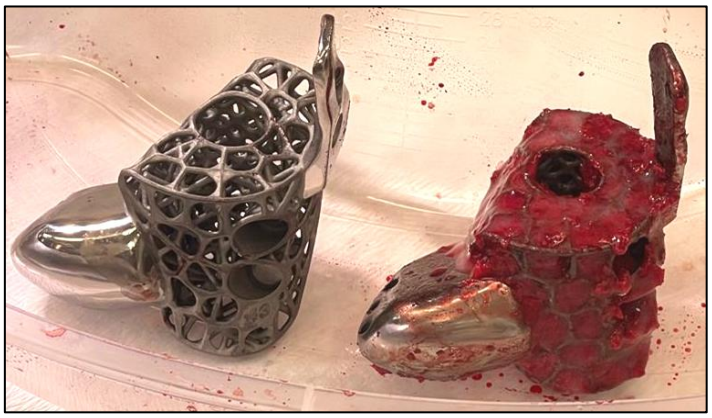

Figure 8. Cage filled with Autologous Bone Graft from RIA followed by Application of Arthrozheal.

2.3. Post Operative Care

Patients were admitted with leg elevation until wound inspection on the third postoperative day where new full cast were applied. Teicoplanin were administered for 3 days before discharge with strict non weight bearing and leg elevation instructions. Deep vein thrombosis prophylaxis in the form of Dalteparin were supplied until patients were able to partial weight bear, typically more than 3 months after surgery. Wound inspection were performed every 2 weeks until fully healed and cast were kept for a minimum of 3 months. Plain radiographs and CT scans were performed at 3 months and 6 months to confirm union before patients were allowed to fully weight bear. Patients were followed up for a minimum of 1 year.

2.4. Data Collection

Information on patient demographics, comorbidities, clinical features, investigations, surgical procedures and outcomes were collected from the hospital electronic data base system. During follow ups, patients were monitored with Visual Analogue Scale (VAS) and American Orthopaedic Foot and Ankle Society(AOFAS) score. They were then given the 36-Item Short Form Survey Instrument (SF-36) and Foot Function Index (FFI) questionnaire to monitor functional outcomes. Radiographic parameters from plain radiographs were documented before and after surgeries to identify degree of correction.

3. Results

Our study involved 6 patients with mean age of 64.3 years (range 59 to 78 years) and consisted of 5 (83.3%) males and 1 (16.7%) female. The body mass index (BMI) average was 29.5 (26.5 to 35.4) with 4 overweight and 2 obese. 3 patients were smokers and 3 were non smokers. 2 patients had peripheral arterial disease (PAD) with involvement at the level of tibioperoneal trunk and posterior tibial artery each. One patient suffered from Charcot neuroarthropathy while 3 (50%) patients had chronic kidney disease. Glycated hemoglobin (HbA1c) levels averaged at 45.6 mmol/mol (range 36-70). Preoperative hemoglobin level mean was 120.5 g/L (range 105-146) while C-reactive protein average was 9.3 (range 6 to 16).

3 (50%) patients suffered from osteomyelitis secondary to infected implants while another 3 (50%) cases involved post traumatic arthritis secondary to avascular necrosis (AVN) of talus. The 3 cases with osteomyelitis underwent 2 stage surgery where the first stage involved removal of implants, methodical debridement and antibiotic cement spacer for at least 3 months before the 3D printed scaffold fixation. The other 3 patients underwent single stage surgery after comfirming absence of infection. With regards to prior surgeries, 1 patient had 5, 2 cases with 3, 1 with single surgery and 2 patients with none. The surgical approach were variable with 2 cases involved medial incision alone, 2 with lateral approach alone and 2 with lateral and dorsomedial approaches. All cases

 doi:10.20944/preprints202504.0044.v1

involved 3D printed keystone talus with 5 included hindfoot nail, 1 total articulating navicular extension with tibial flange, 2 with tibial and navicular flanges and 2 with navicular flange. The keystone cage incorporated custom planned clearance holes for additional screws where 2 additional subtalar screws were done in 5 cases, 2 screws to talus in 1 case, 1 screw to tibia in a case and 1 screw to navicular in 1 case. All cases involved packing of autologous bone graft harvested from RIA followed by PRF application.

The average duration of surgery was 207 minutes (range 162 to 255). None of the patients required blood transfusion. All the patients were admitted for 3 days. The mean duration of complete wound healing is 34.7 days (range 20 to 45 days). All patients (100%) achieved union based on CT scans with mean duration of 20.2 weeks (range 14 to 27 weeks) (Figure 9). All patients were able to ambulate in full weight bearing after average duration of 23.3 weeks (range 16 to 29 weeks). 1 patient sustained superficial wound infection and was treated with oral antibiotics which resolved after 2 weeks. (Table 1)

Table 1. Demonstration of Demography, Surgical Details and Clinical Outcomes.

CASE	1	2	3	4	5	6
Age	62	59	60	60	78	67
Diagnosis	OM	OM	OM	AVN	AVN	AVN
Smoking	No	Yes	Yes	No	Yes	No
BMI	26.5	27.4	27.4	28.2	32.1	35.4
Medical	Nil	IHD, CKD, PAD	CKD	CKD, PAD	DM	IHD, DM, CKD, CN
HbA1c	36	39	39	41	49	70
CRP	8	7	16	9	10	6
Hb (g/L)	113	105	132	146	113	114
Past surgery	5	3	3	0	1	0
Modification	Tibial & Navicular flange, Nail	Navicular flange, Nail	Tibial & Navicular flange	Navicular flange, Nail	Nail	Articulating Navicular extension, Tibial flange, Nail
Duration of surgery (Min)	255	220	162	210	190	205
Wound Healing (Days) - weeks	42	40	20	29	32	45
Union (Weeks)	25	19	16	14	27	20
Ambulation (Weeks)	28	21	18	16	29	22

Abbreviations: OM, Osteomyelitis of Talus; AVN, Avascular Necrosis; BMI, Body Mass Index; IHD, Ischemic Heart Diseasel; CKD, Chronic Kidney Disease; PAD, Peripheral Arterial Disease; DM, Diabetes Mellitus; CN, Charcot Neuroarthropathy.

 doi:10.20944/preprints202504.0044.v1

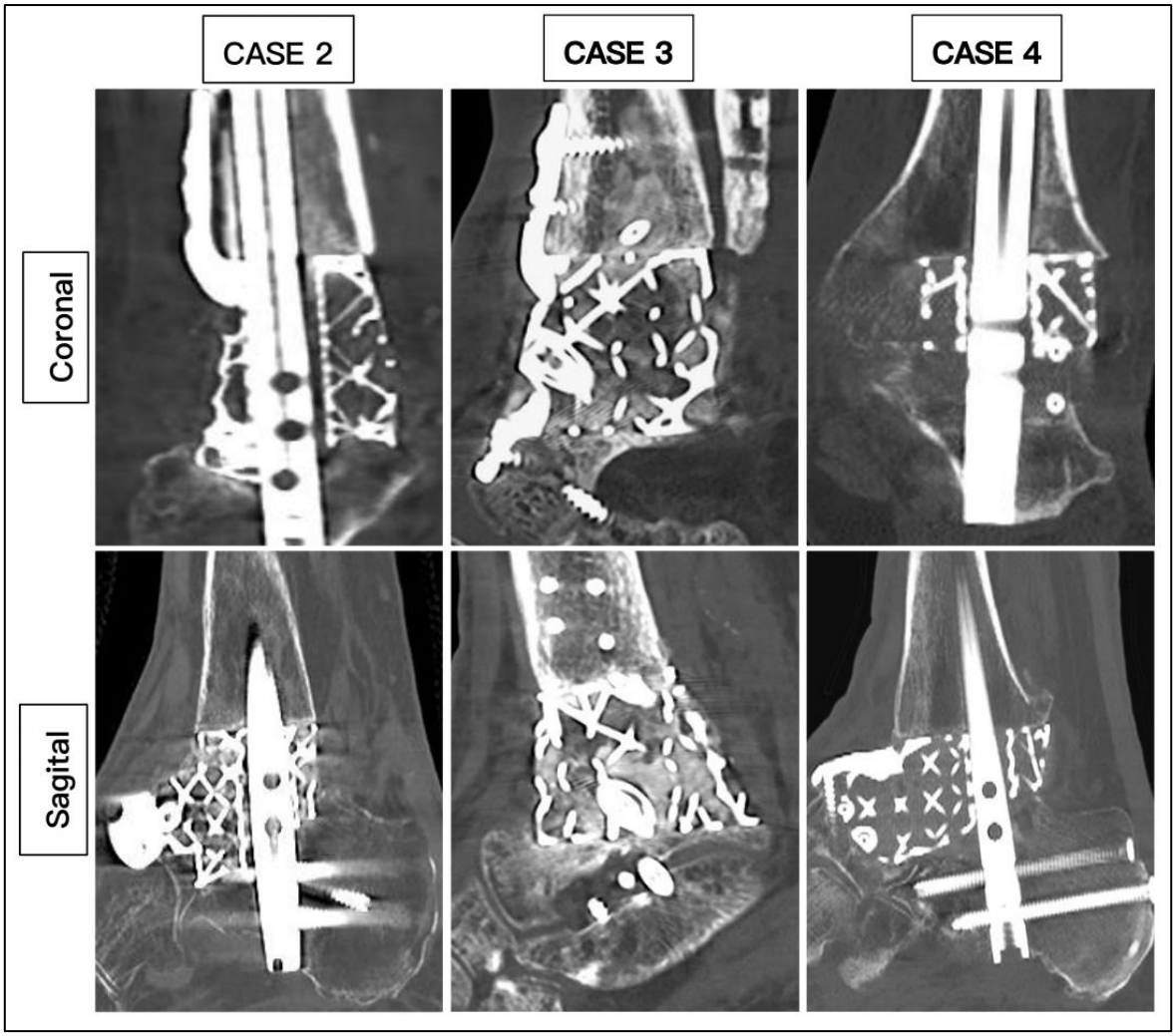

Figure 9. Demonstration of Union from CT scans.

Radiographic measurements were taken pre and post-operatively. (Figures 10 and 11) From the AP radiographs, the preoperative tibiocalcaneal angle, tibiocalcaneal distance, foot height and tibiotalar angle averaged at 14.5 degrees (range 6.8 degrees varus to 38.4 degrees), 25.7 mm (range 6.2 to 53.2), 50.3 mm (range 38.3 to 58.1) and 6.8 degrees (range 6.1 degrees varus to 16.1 degrees) and postoperative mean were 4.5 degrees (range 3.0 to 6.2), 8.0 mm (range 4.8 to 11.7), 56.8 mm (range 50.1 to 74.3) and 0.8 degrees (range 0.2 to 1.4) with difference mean of 14.0 degrees (range 6.3 to 32.0), 20.5 mm (range 9.8 to 44.1), 7.3 mm (range 0.2 to 19.5) and 7.6 degrees (range 0.5 to 12.4). The lateral radiographs revealed average preoperative lateral distal tibia angle, lateral tibiotalar angle, Meary's angle, calcaneal inclination angle, navicular height and plantigrade angle of 88.7 degrees (range 76.6 to 101.5), 84.5 degrees (range 59.1 to 107.6), 9.9 degrees (range 2.3 to 24.1), 19.0 degrees (range 4.7 to 37.1), 34.3 mm (range 17.4 to 44.8) and 88.8 degrees (range 85.1 to 93.7) while postoperative mean were 88.6 degrees (range 85.3 to 92.7), 70.4 degrees (range 67.3 to 72.1), 3.0 degrees (range 1.8 to 5.3), 20.0 degrees (range 14.8 to 22.6), 40.6 mm (range 35.9 to 46.5) and 89.4 degrees (range 86.9 to 92.6) with mean difference of 7.6 degrees (range 0.5 to 12.4), 19.4 degrees (range 4.0 to 40.3), 6.9 degrees (range 0.3 to 18.8), 8.2 degrees (range 0.3 to 16.0), 7.5 mm (range 1.7 to 20.7) and 2.6 degrees (range 0.3 to 5.2). (Table 2)

 doi:10.20944/preprints202504.0044.v1

Figure 10. Demonstration of Plain Radiograph in AP and Lateral Pre and Post Fixation.

 doi:10.20944/preprints202504.0044.v1

Figure 11. Demonstration of Plain Radiograph in AP and Lateral Pre and Post Fixation.

Table 2. Demonstration of Radiographic Parameters Pre and Post Surgery.

CASE	1	2	3	4	5	6
Tibiocalcaneal angle (Pre)	38.4	18.6	12.4	-6.8	13.8	10.5
Tibiocalcaneal angle (Post)	6.2	3.0	3.4	4.2	6.1	4.2
Difference	32.2	15.6	9.0	11	7.7	6.3
Tibiotalar angle (Pre)	16.1	4.4	12.4	-6.1	11.9	2.1
Tibiotalar angle (Post)	1.4	1.2	0.9	0.2	0.5	0.7
Difference	14.7	3.2	11.5	6.3	11.4	2.0

 doi:10.20944/preprints202504.0044.v1

Tibiocalcaneal DIstance (Pre)	53.2	24.0	24.0	6.2	27.7	18.9
Tibiocalcaneal DIstance (Post)	9.1	7.2	4.8	6.0	11.7	9.1
Difference	44.1	16.8	19.2	17.2	16.0	9.8
Foot Height (Pre)	43.8	58.1	54.8	54.1	52.8	38.3
Foot Height (Post)	51.9	58.3	74.3	51.5	54.6	50.1
Difference	8.1	0.2	19.5	2.6	1.8	11.8
Lat Distal Tibial Angle (Pre)	81.2	87.5	76.6	97.7	101.5	87.8
Lat Distal Tibial Angle (Post)	88.9	87	86.6	85.3	91.3	92.7
Difference	7.7	0.5	10.0	12.4	10.2	4.9
Lateral Tibiotalar Angle (Pre)	87.8	67.1	107.6	81.5	103.6	59.1
Lateral Tibiotalar Angle (Post)	69.9	71.1	67.3	72.1	70.8	71.2
Difference	17.9	4.0	40.3	9.4	32.8	12.1
Meary Angle (Pre)	8.0	10.1	2.3	3.2	24.1	11.4
Meary Angle (Post)	3.1	2.0	2.0	1.8	5.3	3.6
Difference	4.8	8.3	0.3	1.4	18.8	7.8
Calcaneal Inclination (Pre)	13.7	37.1	14.5	16.1	27.9	4.7
Calcaneal Inclination (Post)	22.5	21.1	14.8	22.6	22.1	16.7
Difference	8.8	16.0	0.3	6.2	5.8	12
Navicular Height (Pre)	33.1	39.3	44.8	37.5	33.4	17.4
Navicular Height (Post)	41.4	35.9	46.5	41.6	40.1	38.1
Difference	8.3	3.4	1.7	4.1	6.7	20.7
Plantigrade Angle (Pre)	85.1	93.7	86.9	90.0	89.8	87.4
Plantigrade Angle (Post)	86.9	88.7	89.4	89.5	89.5	92.6
Difference	1.8	5.0	2.5	0.5	0.3	5.2

The preoperative VAS and AOFAS scores averaged at 7.5 (range 5 to 9) and 13.5 (range 7 to 27) while postoperative mean were 2.33 (range 1 to 4) and 69 (range 62 to 86) with average improvement of 5.2 (range 4 to 6) and 55.5 (range 51 to 59). The FFI reported preoperative average overall, pain, disability and activity limitation scale at 91.5% (range 83 to 96), 78.7% (range 46 to 100), 96% (range 90 to 100) and 99.5% (range 97 to 100) compared to postoperative mean of 39.3% (range 19 to 51), 24% (range 6 to 32), 50.2% (range 30 to 63) and 31.5% (range 10 to 53) with average improvement of 52.2% (range 45 to 69), 55% (range 26 to 68), 45.8% (range 32 to 70) and 68% (range 47 to 90). The SF-36 reported preoperative average of each domains involving physical functioning, role limitations due to physical health, role limitations due to emotional problems, energy or fatigue, emotional well-being, social functioning, pain and general health of 10% (range 5 to 15), 0%, 11.1% (range 0 to 33.3), 19.2% (range 5 to 35), 23.3 (range 16 to 36), 12.5% (range 0 to 25), 18.3 (range 0 to 45), 20.8% (range 5 to 35) and 20.8 (range 0 to 25) while postoperative mean were 56.7% (range 45 to 85), 54.2% (range 25 to 75), 77.8% (range 66.7 to 100), 65% (range 45 to 80), 75.3% (range 60 to 84), 66.7% (range 50 to 87.5), 79.2 (range 67.5 to 87.5), 69.3% (range 50 to 85) and 87.5% (range 75 to 100) with average improvement of 46.7% (range 40 to 75), 54.2 (range 25 to 75), 66.7% (range 33.4 to 100), 45.8% (range 35 to 60), 52% (range 40 to 68), 54.2% (range 25 to 75), 60.8 (range 42.5 to 77.5), 48.5% (range 41 to 55) and 66.7% (range 50 to 100). (Table 3)

 doi:10.20944/preprints202504.0044.v1

Table 3. Demonstration of Clinical and Functional Outcome Pre and Post Surgery.

CASE	1	2	3	4	5	6	Mean Difference
Pain Score							
VAS pre	8	7	8	9	8	5	5.2±0.8
VAS post	2	1	3	4	3	1	
Functional Score							
AOFAS pre	20	27	8	10	9	7	55.5±3.2
AOFAS post	71	86	63	66	62	66	
FFI (Pre)	93	88	96	95	94	83	52.2±9.1
FFI (Post)	39	19	51	48	41	38	
Pain (Pre)	84	60	88	100	94	46	55.0±14.8
Pain (Post)	26	6	28	32	32	20	
Disability (Pre)	96	100	100	90	92	98	45.8±13.4
Disability (Post)	49	30	63	58	52	49	
AL (Pre)	100	100	100	100	97	100	68.0±15.0
AL (Post)	30	10	53	43	20	33	
Quality of Life (SF-36)							
PF (Pre)	10	10	5	10	10	15	46.7±14.0
PF (Post)	55	85	45	50	50	55	
RP (Pre)	0	0	0	0	0	0	54.2±18.8
RP (Post)	50	75	25	50	50	75	
RE (Pre)	0	33.3	0	0	0	33.3	66.7±21.1
RE (Post)	66.7	100	66.7	66.7	100	66.7	
EF (Pre)	5	35	10	20	10	35	45.8±10.2
EF (Post)	65	80	45	65	65	70	
EW (Pre)	20	36	20	24	24	16	52.0±10.1
EW (Post)	80	84	60	72	72	84	
SF (Pre)	0	25	0	25	12.5	12.5	54.0±17.0
SF (Post)	75	87.5	50	50	75	62.5	
Pain (Pre)	22.5	32.5	0	0	10	45	60.8±15.6
Pain (Post)	67.5	87.5	77.5	77.5	77.5	87.5	
GH (Pre)	30	35	5	15	15	25	49.0±5.8
GH (Post)	71	85	50	70	70	70	

Abbreviations: VAS, Visual Analogue Scale; AOFAS, American Orthopaedic Foot and Ankle Society; FFI, Foot Function Index; AL, Activity Limitation; SF-36, Short Form Health Survey; PF, Physical functioning; RP, Role limitations due to physical health; RE, Role limitations due to emotional problems; EF, Energy/fatigue; EW, Emotional well-being; SF, Social functioning; GH, General health.

4. Discussion

Hindfoot deformities with the presence of non salvageable talus are complex to manage as talus functions as a keystone structure to the ankle. The treatment plan often relies on the architecture of the remaining talus. As patients often present with secondary arthritis to ankle and subtalar arthritis, treatment options becomes severely limited. The emergence of 3D printed scaffold has opened new

 doi:10.20944/preprints202504.0044.v1

options with custom fit cages which accommodate arthrodesis modalities. These custom made implant has been reported to achieve far superior union rate of around 75% compared to femoral head allograft [22].

Union is the most important outcome but the definition of it has been controversial. Traditional use of plain radiographs to define union has not been accurate as it does not correlate with patient's functional outcome. A study comparing the use of radiographs and CT scans reported significant difference with radiographs ambiguously reported much higher union rate [23]. The definition of union based on CT scans is however variable ranging from 25 to 70% of osseous bridging with majority of studies delineate as 50% [24,25]. Additionally, studies reported better clinical outcomes in CT defined osseous bridging of more than 25-50% compared to those below 25% [26]. In our study, we defined union as osseous bridging more than 50% from CT scans with good functional outcome, primarily the ambulatory status.

The reported union rate with the use of 3D printed scaffold for ankle arthrodesis range from 84 to 100% [27,28]. Our study demonstrate similar union rate of 100%. The duration to union has been reported in a systemic review ranging from 4 to 6 months with mean of 5.3 months [29]. Our study demonstrate similar duration to union with average of 20.2 weeks which translates to 4.6 months. Compared to majority of studies where autograft and allograft were used, one study reported union rate of 100% with functional union after 2.6 months with the application of RIA [30]. We postulate that the use of PRF matrix with RIA improve union rate and duration to union.

Despite 3D printed scaffold being a relatively new modality, the reported functional outcomes has been promising. With regards to pain score, most studies reported significant improvement with a study demonstrating reduction of VAS from 6.6 ± 2.9 points to 2.0 ± 1.7 points. Our study reported similar outcome with improvement of VAS from 7.5 ± 1.4 points to 2.3 ± 1.2. Several studies has proclaimed improvement of functional outcome with the use of AOFAS score, FFI and SF-36 in all domains, which is similar to our study [31,32]. There were limited study reporting the degree of correction with one study demonstrating mean coronal correction of 25 degrees and sagittal correction of 6 degrees. [28]. In our present study, we demonstrated similar improvement but included all necessary parameters.

We acknowledge that there are several limitations to our study. This is a retrospective study describing the use of a single technique which is the PRF coated 3D printed scaffold in managing complex hindfoot deformities with significant bony defects. A comparative study would be more significant in reflecting clinical outcomes. Due to the rarity of such cases and this modality being relatively new, the sample size was limited. Longer follow-up duration would improve the assessment of long-term outcomes.

5. Conclusions

This study intends to demonstrate the potential of PRF coated 3D printed scaffold in managing complex hindfoot cases especially in the presence of significant bone defects. This modality demonstrated optimal union rate of 100%, near anatomical correction and good functional outcomes with low complication rate. The addition of PRF enhances union rate and time for complete osteointegration. Further comparative studies with larger number of patients is required to determine statistical significance to improve quality of care for such cases.

Author Contributions: Conceptualisation A.P; Data collection: K.T. and J.M; Writing, literature review and editing: K.T.; Supervision: A.P. All authors have read and agreed to the published version of the manuscript.

Funding: This research received no external funding.

Institutional Review Board Statement: This study has been approved by Department of Clinical Audit with ID 920618125. Discussion with the Hospital Trust Research & Innovation Department, and using the NHS Health Research Authority's online tool, the project was deemed to be a service evaluation. Further ethical approval was not required as patients' management was not affected in any way and treatment had already been provided.

 doi:10.20944/preprints202504.0044.v1

Informed Consent Statement: Not applicable as the study was a retrospective evaluation of clinical outcomes.

Data Availability Statement: No data is provided due to privacy restrictions.

Acknowledgments: The authors are grateful to all patients and the staffs at the Wythenshawe Hospital, Manchester University NHS Foundation Trust (MFT) who contributed to the management of patients.

Conflicts of Interest: The authors declare no conflicts of interest.

References

1. Shono, H.; Matsumoto, Y.; Kokubun, T.; Tsuruta, A.; Miyazawa, T.; Kobayashi, A.; Kanemura, N. Determination of Relationship between Foot Arch, Hindfoot, and Hallux Motion Using Oxford Foot Model: Comparison between Walking and Running. Gait & Posture 2022, 92, 96–102. https://doi.org/10.1016/j.gaitpost.2021.10.043.
2. Chatterton, B. D.; Muller, S.; Roddy, E. Epidemiology of Posterior Heel Pain in the General Population: Cross-Sectional Findings from the Clinical Assessment Study of the Foot. Arthritis Care & Research 2015, 67 (7), 996–1003. https://doi.org/10.1002/acr.22546.
3. Adelaar, R. S.; Madrian, J. R. Avascular Necrosis of the Talus. Orthopedic Clinics of North America 2004, 35 (3), 383–395. https://doi.org/10.1016/j.ocl.2004.02.010.
4. Jordan, R. K.; Bafna, K. R.; Liu, J.; Ebraheim, N. A. Complications of Talar Neck Fractures by Hawkins Classification: A Systematic Review. The Journal of Foot and Ankle Surgery 2017, 56 (4), 817–821. https://doi.org/10.1053/j.jfas.2017.04.013.
5. Stake, I. K.; Madsen, J. E.; Hvaal, K.; Johnsen, E.; Husebye, E. E. Surgically Treated Talar Fractures. A Retrospective Study of 50 Patients. Foot and Ankle Surgery 2015, 22 (2), 85–90. https://doi.org/10.1016/j.fas.2015.05.005.
6. Vints, W.; Matricali, G.; Geusens, E.; Nijs, S.; Hoekstra, H. Long-Term Outcome after Operative Management of Talus Fractures. Foot & Ankle International 2018, 39 (12), 1432–1443. https://doi.org/10.1177/1071100718790242.
7. Clement, R. G. E.; Wong, S. J.; Hall, A.; Howie, S. E. M.; Simpson, A. H. R. W. The Long-Term Time Course of Septic Arthritis. Bone & Joint Open 2024, 5 (9), 785–792. https://doi.org/10.1302/2633-1462.59.bjo-2024-0048.r1.
8. Kim, H.; Bae, S.-Y. Talus Osteomyelitis by Candida Krusei with Multiple Huge Cystic Lesions: A Case Report and Review of Literatures. BMC Musculoskeletal Disorders 2022, 23 (1). https://doi.org/10.1186/s12891-022-05648-4.
9. Winkler, E.; Schöni, M.; Krähenbühl, N.; Uçkay, I.; Waibel, F. W. A. Foot Osteomyelitis Location and Rates of Primary or Secondary Major Amputations in Patients with Diabetes. Foot & Ankle International 2022, 107110072210885. https://doi.org/10.1177/10711007221088552.
10. Eschler, A.; Gradl, G.; Wussow, A.; Mittlmeier, T. Prediction of Complications in a High-Risk Cohort of Patients Undergoing Corrective Arthrodesis of Late Stage Charcot Deformity Based on the PEDIS Score. BMC Musculoskeletal Disorders 2015, 16 (1). https://doi.org/10.1186/s12891-015-0809-6.
11. Leslie, M. D.; Schindler, C.; Rooke, G. M. J.; Dodd, A. CT-Verified Union Rate Following Arthrodesis of Ankle, Hindfoot, or Midfoot: A Systematic Review. Foot & Ankle International 2023, 44 (7), 665–674. https://doi.org/10.1177/10711007231171087.
12. Miniaci-Coxhead, S. L.; Weisenthal, B.; Ketz, J. P.; Flemister, A. S. Incidence and Radiographic Predictors of Valgus Tibiotalar Tilt after Hindfoot Fusion. Foot & Ankle International 2017, 38 (5), 519–525. https://doi.org/10.1177/1071100717690439.
13. Xu, W.; Liu, Z.; Lu, X.; Tian, J.; Chen, G.; Liu, B.; Li, Z.; Qu, X.; Wen, C. Porous Ti-10Mo Alloy Fabricated by Powder Metallurgy for Promoting Bone Regeneration. Science China Materials 2019, 62 (7), 1053–1064. https://doi.org/10.1007/s40843-018-9394-9.
14. Mayfield, C. K.; Ayad, M.; Lechtholz-Zey, E.; Chen, Y.; Lieberman, J. R. 3D-Printing for Critical Sized Bone Defects: Current Concepts and Future Directions. Bioengineering 2022, 9 (11), 680. https://doi.org/10.3390/bioengineering9110680.

 doi:10.20944/preprints202504.0044.v1

15. Hallman, M.; Driscoll, J. A.; Lubbe, R.; Jeong, S.; Chang, K.; Haleem, M.; Jakus, A.; Pahapill, R.; Yun, C.; Shah, R.; Hsu, W. K.; Stock, S. R.; Hsu, E. L. Influence of Geometry and Architecture on the in Vivo Success of 3D-Printed Scaffolds for Spinal Fusion. Tissue Engineering Part A 2020, 27 (1-2), 26–36. https://doi.org/10.1089/ten.tea.2020.0004.
16. Schemitsch, E. H. Size Matters. Journal of Orthopaedic Trauma 2017, 31, S20–S22. https://doi.org/10.1097/bot.0000000000000978.
17. Dekker, T. J.; Steele, J. R.; Federer, A. E.; Hamid, K. S.; Adams, S. B. Use of Patient-Specific 3D-Printed Titanium Implants for Complex Foot and Ankle Limb Salvage, Deformity Correction, and Arthrodesis Procedures. Foot & Ankle International 2018, 39 (8), 916–921. https://doi.org/10.1177/1071100718770133.
18. Abar, B.; Kwon, N.; Allen, N. B.; Lau, T.; Johnson, L. G.; Gall, K.; Adams, S. B. Outcomes of Surgical Reconstruction Using Custom 3D-Printed Porous Titanium Implants for Critical-Sized Bone Defects of the Foot and Ankle. Foot & Ankle International 2022, 107110072210771. https://doi.org/10.1177/10711007221077113.
19. Wallace, N.; Schaffer, N. E.; Aleem, I. S.; Patel, R. 3D-Printed Patient-Specific Spine Implants. Clinical Spine Surgery: A Spine Publication 2020, Publish Ahead of Print. https://doi.org/10.1097/bsd.0000000000001026.
20. Pavlovic, V.; Ciric, M.; Jovanovic, V.; Trandafilovic, M.; Stojanovic, P. Platelet-Rich Fibrin: Basics of Biological Actions and Protocol Modifications. Open Medicine 2021, 16 (1), 446–454. https://doi.org/10.1515/med-2021-0259.
21. Tahsin Beyzadeoğlu; Tuna Pehlivanoğlu; Kerem Yıldırım; Halil Buldu; Tandoğan, R. N.; Ümit Tüzün. Does the Application of Platelet-Rich Fibrin in Anterior Cruciate Ligament Reconstruction Enhance Graft Healing and Maturation? A Comparative MRI Study of 44 Cases. Orthopaedic Journal of Sports Medicine 2020, 8 (2), 232596712090201-232596712090201. https://doi.org/10.1177/2325967120902013.
22. Steele, J. R.; Kadakia, R. J.; Cunningham, D. J.; Dekker, T. J.; Kildow, B. J.; Adams, S. B. Comparison of 3D Printed Spherical Implants versus Femoral Head Allografts for Tibiotalocalcaneal Arthrodesis. The Journal of Foot and Ankle Surgery: Official Publication of the American College of Foot and Ankle Surgeons 2020, 59 (6), 1167–1170. https://doi.org/10.1053/j.jfas.2019.10.015.
23. Coughlin, M. W.; Grimes, J. S.; Traughber, P. D.; Jones, C. P. Comparison of Radiographs and CT Scans in the Prospective Evaluation of the Fusion of Hindfoot Arthrodesis. 2006, 27 (10), 780–787. https://doi.org/10.1177/107110070602701004.
24. Krause, F.; Younger, A. S. E.; Baumhauer, J. F.; Daniels, T. R.; Glazebrook, M.; Evangelista, P. T.; Pinzur, M. S.; Thevendran, G.; Donahue, R. M. J.; DiGiovanni, C. W. Clinical Outcomes of Nonunions of Hindfoot and Ankle Fusions. The Journal of bone and joint surgery. American volume 2016, 98 (23), 2006–2016. https://doi.org/10.2106/JBJS.14.00872.
25. Aubret; Merlini, L.; M. Fessy; Besse, J.-L. Poor Outcomes of Fusion with Trabecular Metal Implants after Failed Total Ankle Replacement: Early Results in 11 Patients. Orthopaedics & Traumatology Surgery & Research 2018, 104 (2), 231–237. https://doi.org/10.1016/j.otsr.2017.11.022.
26. Glazebrook, M.; Beasley, W.; Daniels, T.; Evangelista, P. T.; Donahue, R.; Younger, A.; Pinzur, M. S.; Baumhauer, J. F.; DiGiovanni, C. W. Establishing the Relationship between Clinical Outcome and Extent of Osseous Bridging between Computed Tomography Assessment in Isolated Hindfoot and Ankle Fusions. Foot & Ankle International 2013, 34 (12), 1612–1618. https://doi.org/10.1177/1071100713504746.
27. Strydom, A.; Saragas, N. P.; Ferrao, P. N. The Use of a 3D Printed Titanium Implant for Arthrodesis in the Management of Large Osseous Defects in the Ankle. Foot and Ankle Surgery 2023, 29 (8), 576–583. https://doi.org/10.1016/j.fas.2023.05.005.
28. Kim, M. S.; Mann, T.; Kelly, C.; Palmer, R. C.; Abar, B.; Zhang, H.; Cush, G. J. Mid-Term Outcomes of Lower Limb Salvage with 3D-Printed Ankle Cages. Foot & Ankle Surgery: Techniques, Reports & Cases 2024, 4 (3), 100413. https://doi.org/10.1016/j.fastrc.2024.100413.
29. Schick, V. D.; Zampogna, B.; Marrara, G.; Siracusano, L.; Larizza, L.; Calaciura, S.; Sanzarello, I.; Marinozzi, A.; Leonetti, D. Custom-Made 3D-Printed Titanium Implants for Managing Segmental Distal Tibial Bone Defects: A Systematic Literature Review. Journal of Clinical Medicine 2025, 14 (6), 1796. https://doi.org/10.3390/jcm14061796.

 doi:10.20944/preprints202504.0044.v1

30. Hammaad Gamieldien; Ferreira, N.; Franz Friedrich Birkholtz; Hilton, T.; Campbell, N.; Laubscher, M. Filling the Gap: A Series of 3D-Printed Titanium Truss Cages for the Management of Large, Lower Limb Bone Defects in a Developing Country Setting. European Journal of Orthopaedic Surgery & Traumatology 2022, 33 (3), 497–505. https://doi.org/10.1007/s00590-022-03434-5.
31. Lewis, T. L.; Walker, R.; Alkhalfan, Y.; Latif, A.; Abbasian, A. Custom Patient-Specific 3D-Printed Titanium Truss Tibiotalocalcaneal Arthrodesis Implants for Failed Total Ankle Replacements: Classification, Technical Tips, and Treatment Algorithm. Foot & Ankle International 2024, 45 (9), 950–961. https://doi.org/10.1177/10711007241255381.
32. Eamon Ramhamadany; Chadwick, C.; Davies, M. B. Treatment of Severe Avascular Necrosis of the Talus Using a Novel Keystone-Shaped 3D-Printed Titanium Truss Implant. Foot & ankle orthopaedics 2021, 6 (4). https://doi.org/10.1177/24730114211043516.